

Output characteristics of SASE-driven short wavelength FEL's

William M. Fawley

Lawrence Berkeley National Laboratory, MS 47-112
1 Cyclotron Road
Berkeley, CA 94720

ABSTRACT

This paper investigates various properties of the “microspikes” associated with self-amplified spontaneous emission (SASE) in a short wavelength free-electron laser (FEL). Using results from the 2-D numerical simulation code GINGER, we confirm theoretical predictions such as the convective group velocity in the exponential gain regime. In the saturated gain regime beyond the initial saturation, we find that the average radiation power continues to grow with an approximately linear dependence upon undulator length. Moreover, the spectrum significantly broadens and shifts in wavelength to the redward direction, with $P(\omega)$ approaching a constant, asymptotic value. This is in marked contrast to the exponential gain regime where the spectrum steadily narrows, $P(\omega)$ grows, and the central wavelength remains constant with z . Via use of a spectrogram diagnostic $S(\omega, t)$, it appears that the radiation pattern in the saturated gain regime is composed of an ensemble of distinct “sinews” whose widths $\Delta\lambda$ remain approximately constant but whose central wavelengths can “chirp” by varying a small extent with t .

Keywords: Free-electron laser, SASE, x-ray FEL, numerical simulation

1. INTRODUCTION

Over the past six or so years there has been increasing interest at multiple institutions and laboratories concerning the possibility of building single-pass, extremely short wavelength free-electron lasers (FEL's) whose initial radiation is generated by the process of self-amplified stimulated emission (SASE) acting upon shot noise. Unlike FEL's based upon either oscillator configurations, where slippage and detuning effects over hundreds of passes generally clean up the signal and generates a single-mode output, or single-pass master oscillator power amplifier (MOPA) configurations, where the input signal is temporally and spatially coherent, the input signal - random “shot noise” electron beam bunching - in SASE FEL's is neither spatially nor temporally coherent. As was recognized relatively early in FEL history,¹⁻³ the finite spectral bandpass of exponential gain causes the initially broad band shot noise signal to narrow with z . This narrowing continues until a minimum spectral width is reached at the end of the exponential gain regime. More recent work⁴ analyzed the different characteristics of SASE in the short- and long-pulse regimes corresponding to the electron beam length l_b being shorter or much longer, respectively, than l_c , the so-called “cooperation” length. $l_c \equiv \lambda_s/4\pi\rho$, where ρ is the Pierce parameter, is equivalent to the slippage length accumulated over two exponential gains lengths in power and is sometimes also referred to as the coherence length. One of the more interesting predictions both theoretically and from numerical simulation has been that in the time domain the FEL radiation will be composed of a series of high intensity “microspikes” whose characteristic length and separation is $\sim l_c$.

Numerical simulation studies⁴⁻⁷ have confirmed many of the predictions of SASE theory on *macroscopic* time scales (*i.e.* $\tau \gg l_c/c$) such as the effective input signal strength, the narrowing of RMS spectral width versus z together with the corresponding growth of the autocorrelation time, and the average saturation power. Relatively little work has been done concerning radiation properties on the *microscopic* time scale of individual spikes, apart from confirming that the RMS intensity fluctuation $(\langle I^2 \rangle - \langle I \rangle^2)^{1/2} \sim \langle I \rangle$. For example, little is known concerning the spectral characteristics of the individual spikes (*e.g.*, the presence or non-presence of chirping) and the variation of properties such as central wavelength from one spike to another. Nor has there been close examination of the differences between the spectral characteristics of microspikes in the exponential gain regime and those in the saturated gain regime. For many applications which employ the total picosecond-long radiation pulse, details of the femtosecond microspikes may be irrelevant. However, for those applications that require or can exploit the short duration microspikes, their individual spectral characteristics may be quite important.

Further author information: E-mail: fawley@lbl.gov

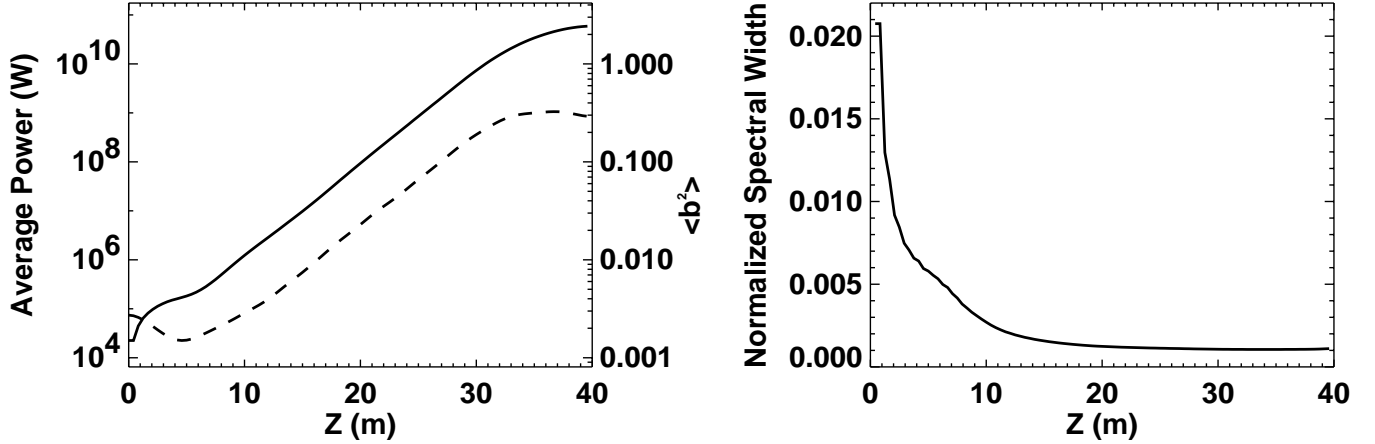


Figure 1. Results from a 2-D GINGER run starting from short noise using LCLS parameters of Table 1. The left plot shows the average radiation power (solid line) and the average electron beam bunching fraction squared as functions of undulator length z . The plot on the right shows the normalized RMS spectral width $\Delta\lambda/\lambda_o$.

This paper examines microspike characteristics for SASE x-ray FEL's, with a particular focus on the proposed “Linac Coherent Light Source” (LCLS) device⁸ which would operate in the 0.1 – 1.0 nm x-ray wavelength region employing the SLAC linac electron beam. In Sec. 2 we discuss the relevant LCLS parameters and the numerical FEL simulation code GINGER. Sec. 3 presents GINGER results for the exponential gain regime from a full 2-D simulation while Sec. 4 examines those from a 1-D simulation of a very long undulator operating primarily in the saturated gain regime. Sec. 5 details some concluding remarks.

2. ADOPTED LCLS PARAMETERS AND THE GINGER FEL SIMULATION CODE

We have chosen a high current ($I_b = 5$ kA), high energy ($E_b = 15$ GeV, instantaneous $\Delta E/E = 3 \times 10^{-4}$), low emittance ($\varepsilon_n \sim 1.5$ mm-mrad, RMS) electron beam together with a helically-polarized, high field ($B \approx 0.98$ T, $a_w = 2.744$), short wavelength ($\lambda_w = 30$ nm) magnetic undulator. Additional, axisymmetric focusing is presumed to bring the betatron wavelength down to 22.4 m and the equilibrium, RMS electron beam radius to $15.6 \mu\text{m}$. With these choices, the effective energy spread due to emittance is $\approx 1.3 \times 10^{-3}$ and nominal $\rho \approx 1.5 \times 10^{-3}$. Note that current plans for the LCLS are concentrating on somewhat lower current electron beams and linearly-polarized undulator fields as would be obtainable from a more conventional, hybrid wiggler. Nonetheless, for our numerical simulation study, these differences show up mainly in the form of decreasing ρ and consequently increasing the exponential gain length.

GINGER⁹ is a 2-D, axisymmetric, ($r - z$), time-dependent, PIC simulation code whose model includes electron beam shot noise, betatron motion, instantaneous energy spread, and slippage, together with radiation gain, diffraction and refraction. Two types of LCLS simulations are presented here. The first is a full 2-D simulation of a 40-m, untapered undulator adopting periodic (in time) boundary conditions with $l_b = 533$ nm $\approx 2.7 l_{\text{slippage}}$ where $l_{\text{slippage}} \equiv z \times (\lambda_s/\lambda_w)$. Since the expected SLAC micropulse length of $\sim 300 \mu\text{m}$ is much longer than l_{slippage} at x-ray wavelengths (and much, much greater than the slippage accumulated over one gain length), periodic boundary conditions should not unduly influence the results. The electron beam and radiation were temporally divided into 256 slices, leading to an effective spacing of 2.1 nm in the laboratory frame. The nominal cooperation length was 9.2 nm, although as discussed in Sec. 3, 2-D effects reduce the gain and increase l_c to ≈ 22 nm.

The second set of simulations concentrated upon the saturated gain regime and adopted an (absurdly) long, untapered wiggler of 120 m. To reduce storage and computation time, we used GINGER in a 1-D mode (no radial dependence) in which diffractive effects are suppressed and the electron beam emittance was reduced three-fold. Here l_b was set equal to $l_{\text{slippage}} = 600$ nm. The effective interslice spacing of 2.3 nm is now somewhat closer to the effective l_c of 13 nm.

3. 2-D EXPONENTIAL GAIN REGIME RESULTS

The 2-D LCLS simulation required ≈ 35 m of undulator to reach a saturated radiation power of ≈ 40 GW when started from shot noise. Figure 1 displays time-averaged laser power, bunching fraction (*squared* in order to illustrate that P and $\langle b^2 \rangle$

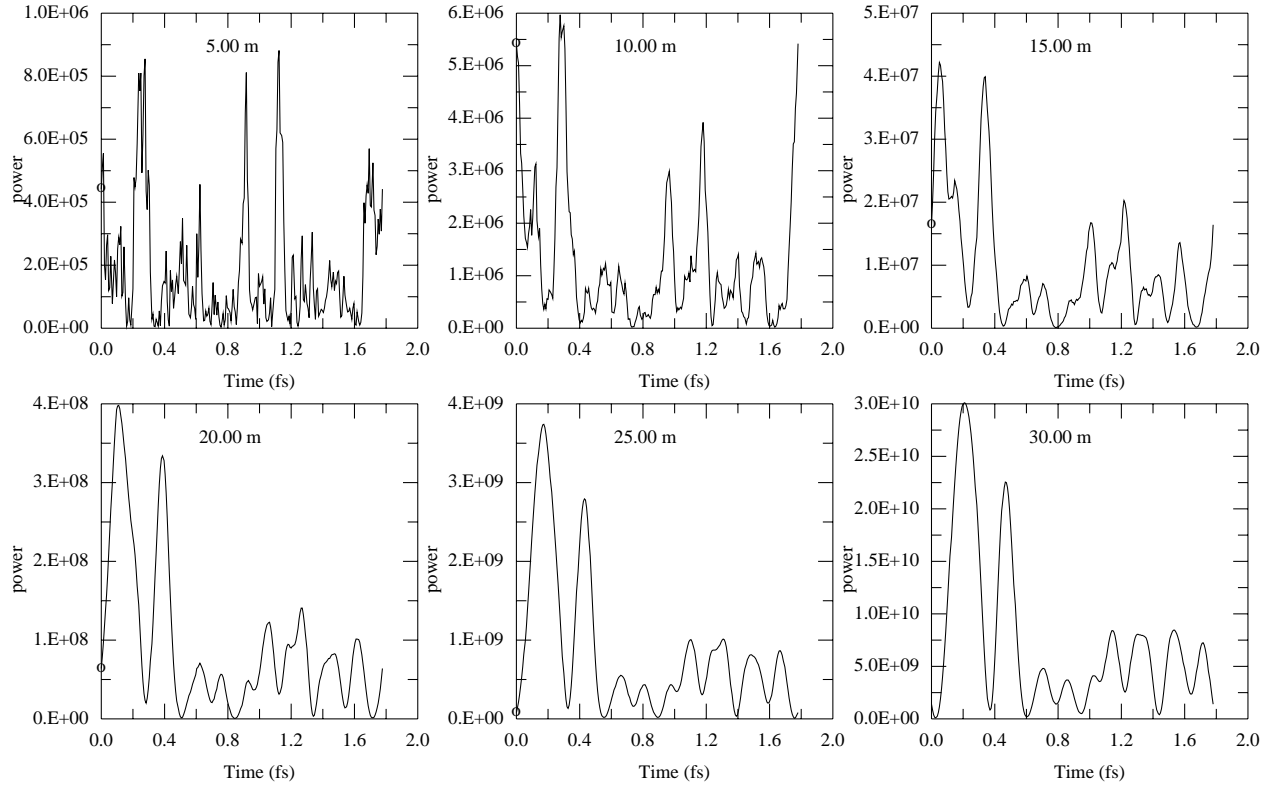


Figure 2. Snapshots of instantaneous power versus time at six z locations for the 2-D GINGER run of Fig. 1.

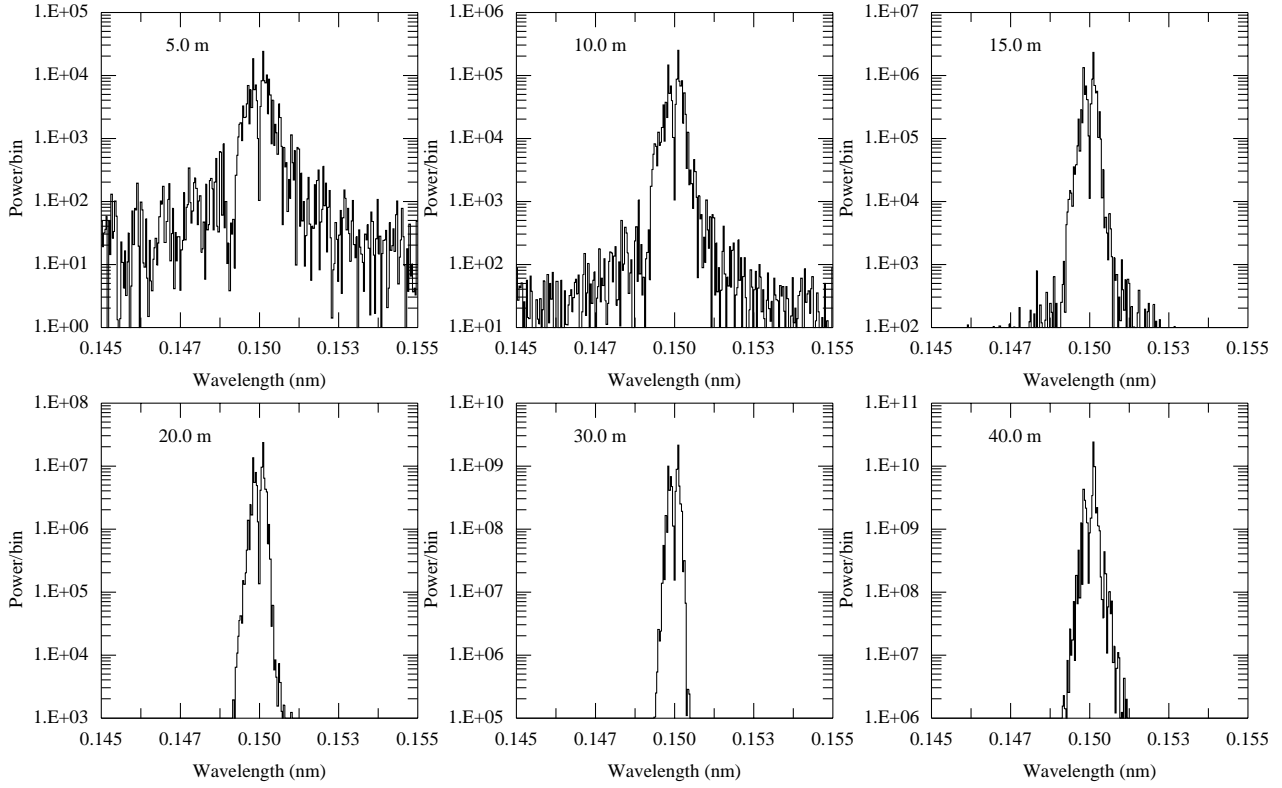


Figure 3. Snapshots of power spectra plotted versus wavelength at six z -locations.

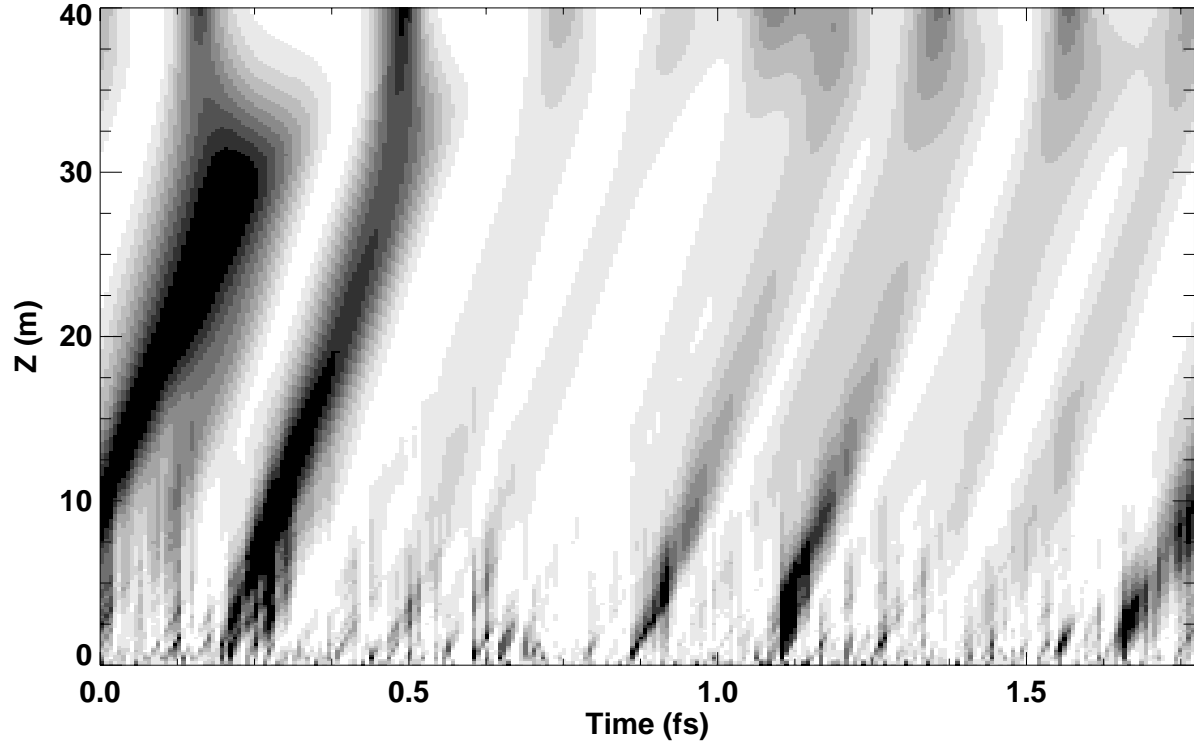


Figure 4. Plot of the normalized instantaneous power, $P(t, z) / \langle P \rangle (z)$, versus time and z for a 40-m long LCLS undulator with relevant electron beam and wiggler parameters given in Sec. 2. The contour levels range from 0.0 (white) to 4.0 (black).

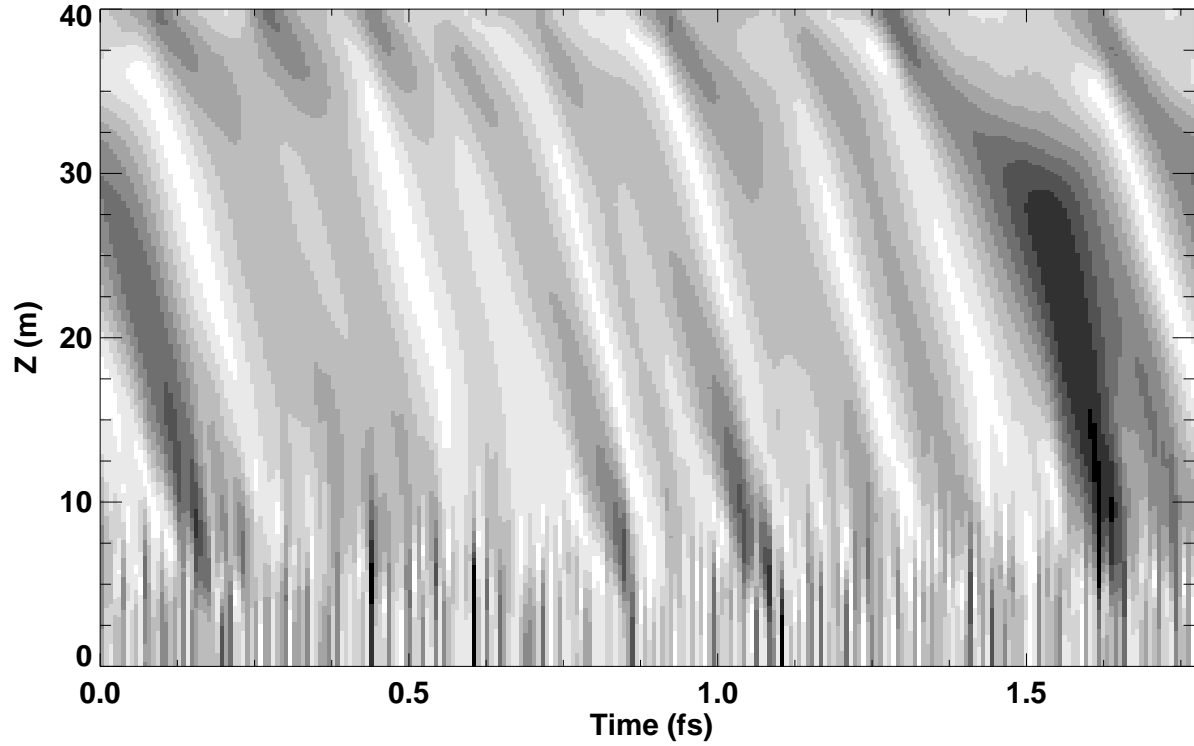


Figure 5. Plot of the normalized instantaneous bunch, $b(t, z) / \langle b \rangle (z)$, versus time and z for the same GINGER simulation shown in 4. The contour levels here range from zero to 3.0.

have the same gain lengths), and normalized spectral width versus z . One sees that the effective input power due to shot noise is ≈ 20 kW. The exponential gain length (in power) is ≈ 2.2 m, corresponding to an effective $\rho = 5.3 \times 10^{-4}$, about 40% of the nominal 1-D theoretical value. The value of power at saturation agrees well with the predicted value of ρP_b while the spectral width of $\approx 1.2 \times 10^{-3}$ agrees better with the 1-D value of ρ than with the 2-D effective value.

Figure 2 shows snapshots of the time-resolved power at six different z -locations. At $z = 5$ m, which is approximately where the asymptotic exponential gain begins to dominate, one observes a small number of high intensity microspikes sitting on top of an extremely noisy base. As z increases, this pattern coalesces into a set of approximately 8 microspikes which maintain their individual identities and their relative amplitudes (more or less) through the end of the simulation.

Figure 3 plots the radiation spectrum on a semi-logarithmic scale at six longitudinal positions. One sees that as the power grows with z , its spectrum steadily narrows until a minimum width occurs around $z \approx 30$ m after which some broadening is seen by $z = 40$ m. One should remember that the fine details of the spectra depend upon the particular set of random numbers adopted for the shot noise start - if a large number of simulations with different seeds were to be averaged (or alternatively a very long electron beam were to be modeled), $P(\omega)$ would approach a smooth, Gaussian-like curve.⁷

Close inspection of the $P(t)$ plots in Fig. 2 shows that microspike pattern is slowly drifting rightwards in time (*i.e.* increasing t with increasing z). This effect, which is related to similar behavior in multi-pass FEL oscillators where the radiation group velocity v_g is also slightly less than c , was predicted by Bonfaccio *et al.*⁴ in their SASE analysis. The drift shows up far more clearly in Fig. 4 which plots contours of the normalized instantaneous power ($\equiv P(t, z) / \langle P \rangle(z)$). The effective drift rate, 9.7×10^{-3} ps/m, is close to the predicted value of 11.1×10^{-3} ps/m, two-thirds of the slippage rate $\propto (1 - v_b/c)$. Beyond saturation at $z \approx 35$ m, the contour pattern becomes vertical indicating that v_g speeds up to c .

A related drift, but here in the opposite direction because it is plotted in time relative to the electron beam longitudinal velocity (which is less than c), appears in Fig. 5, which shows contours of the normalized electron beam bunching $b(t, z) / \langle b \rangle(z)$. At and beyond saturation, the drift rate of the bunching pattern increases to that corresponding to the radiation-electron beam slippage rate, indicating that the bunching pattern and radiation microspikes now both move with $v_g = c$.

One additional item of interest appears when one examines the regions in Figs. 4 and 5 between $z = 0$ and $z \approx 5$ m. Here there is a great deal of high frequency (temporally) noise due to the initial shot noise start. Many of these features do not coalesce into lower frequency microspikes and, instead, propagate vertically (*i.e.* with $v_g = v_b$ for the electron beam bunching and $v_g = c$ for the radiation) on these two plots. These features are almost certainly incoherent undulator radiation produced by shot noise bunching components whose effective central wavelength lies outside the gain bandpass and thus cannot grow in absolute terms. Both the bunching and radiation features eventually “disappear” at larger z on the plots because their amplitudes decrease relative to those microspikes whose central wavelengths do lie within the gain bandpass. This phenomenon may have some practical significance. If, as some have proposed, one filters the SASE radiation at some early point in the undulator in an attempt to narrow the output spectrum, the *unfiltered* electron beam will still produce a broadband spectrum, some of which will lie within the gain bandpass. Thus, the filtering must be done many ($\geq 5 - 8$) gain lengths from the undulator entrance in order that the filtered radiation mode can dominate the unfiltered and untamed shot noise.

4. 1-D SATURATED GAIN REGIME RESULTS

One of the more interesting predictions by Bonifacio *et al* [4] in their examination of SASE in the long pulse limit ($l_b \gg l_c$) was that the radiation power would continue to grow beyond its “first” saturation value at the end of the exponential gain regime. Their paper presented some 1-D simulation results confirming this result (see their Fig. 2). Completely independent, 1-D GINGER runs using LCLS parameters also agree with their prediction. Two 1-D runs with different initial conditions were done: a) an initial signal arising solely from shot noise and b) radiation initialized as a random phase, flat $P(\omega)$ signal with no electron beam shot noise. The two runs gave nearly identical results for the growth of radiation power versus z and average bunching fraction versus z (Fig. 6). The “first” saturation with $P \approx 100$ GW occurs at $z \approx 20$ m followed by a 3.5-fold, growth of the average power over the next 100 m of undulator length. As suggested by Bonifacio *et al.*, there may be an asymptotic “second” saturation whose power is approximately four-times that of the usual “first” saturation at the end of the exponential gain regime (although these runs were too short to reach that limit). Together with the growth in power in the saturated gain regime is a simultaneous slow decrease in bunching fraction from a peak of 0.7 down to a value less than 0.1.

Examination of the plots of instantaneous power versus time (Fig. 7) shows that after the end of the exponential gain regime, the microspike structure begins to get more “noisy” with z , in contrast to the behavior before “first” saturation where $P(t)$ gets smoother with increasing z (*e.g.* Fig. 1). It appears that the overall growth of average power with z in the saturated gain

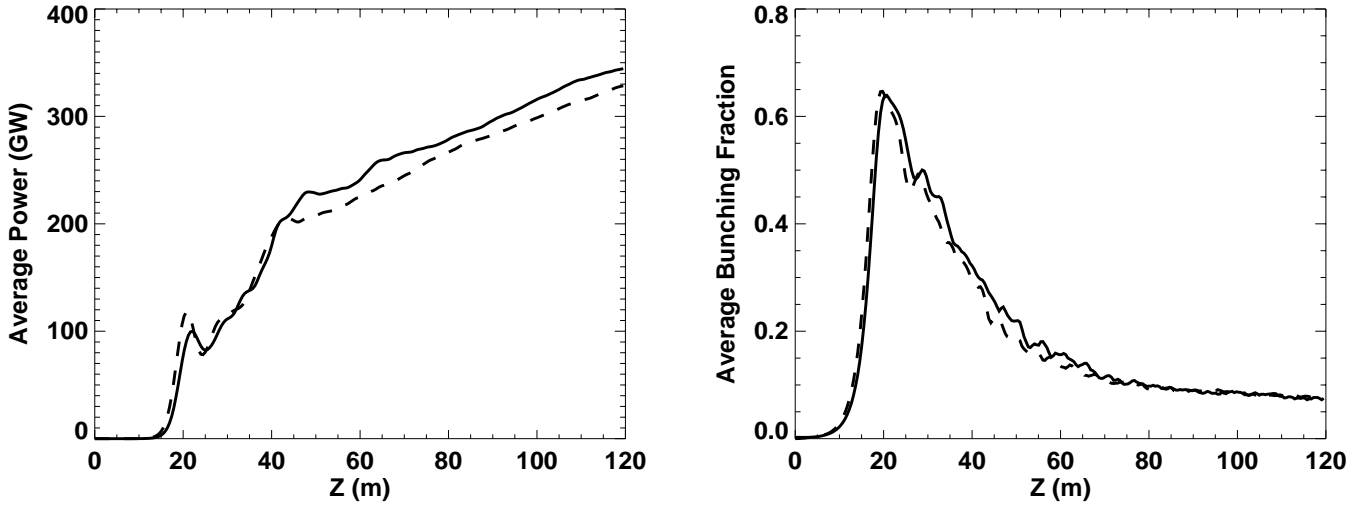


Figure 6. Average power and bunching fraction versus z for two 1-D LCLS-like GINGER simulation run. The solid line is from a run with a shot noise start while the dotted line is from a constant $P(\omega)$ (*i.e.* broadband spectrum) start with no shot noise.

regime may be due to the increase in both the average peak intensity of each microspike and an increase in the number of spikes overcoming a significant narrowing (in the time domain) of the average width.

Associated with this narrowing in the time domain is a steady widening and shift redwards of the overall radiation spectrum (Fig. 8). The shift is presumably due to the average beam electron energy decreasing with z . Close examination of Fig. 8 shows that as the centroid shifts redward, radiation emitted at the original resonance wavelength of 0.150 nm becomes absorbed, dropping in intensity from approximately 10 GW/bin at $z = 40$ m to a few GW/bin at $z = 120$ m. The time-averaged output power of 350 GW at $z = 120$ m corresponds to an 0.45% average energy extraction from the electron beam which would agree with the apparent increase in resonant wavelength from 0.150 to about 0.152 nm. It is also apparent in these plots that the power per spectral bin [and thus $P(\omega)$] reaches an asymptotic value of 10 – 15 GW, in contrast to the behavior in the time domain where the maximum microspike intensity increases from 200 to 1600 GW.

One of the more interesting ways to visualize the radiation data is to produce a spectrogram $S(\omega, \tau)$ which allows one to detect phenomena such as frequency chirping [which is unobservable in a simple $P(\omega)$ plot]. In recent years, a number of groups interested in ultrashort laser pulses have been experimentally producing spectrograms using methods such as frequency-resolved optical gating (FROG; see, *e.g.*, Ref. [10] and references therein). Given that one has intensity and phase information from a simulation code such as GINGER for “all” times at a given z , one can numerically form a simple spectrogram (although one can also extract any of the various FROG “geometries” too):

$$S(\omega, \tau) \equiv \left| \int dt E(t) W(t - \tau) \exp(i\omega t) \right|^2.$$

Here $E(t)$ is the complex field and the weighting function $W(t - \tau)$ was chosen to be a simple one-dimensional Gaussian with a width $\sigma \approx 0.08l_b$.

When plotted on a logarithmic scale such as in Fig. 9, the observer is struck by the appearance of discrete “sinews” running up and down in time, slowly changing intensity, and, in some cases, with central wavelengths oscillating with time (*i.e.* chirping). The overall five-fold broadening in spectrum from $z = 20$ m to $z = 120$ m is accompanied by an increase in the number of sinews, rather than a broadening of a fixed number of such sinews. The typical width $\Delta\lambda$ of each sinew appears to be very close to the value $\rho\lambda_o$, so perhaps one can think of each sinew as a new mode that is able to grow because of the overall reduction in electron beam energy. Hence, each high intensity microspike in the temporal domain is likely the result of constructive interference of a number of discrete sinews in the frequency domain, with the narrowing with z of the microspikes due to constant addition of additional sinews to the redward side of the spectrum. Similar behavior may occur in an untapered, single pass amplifier in a MOPA configuration when sideband growth becomes nonlinear.

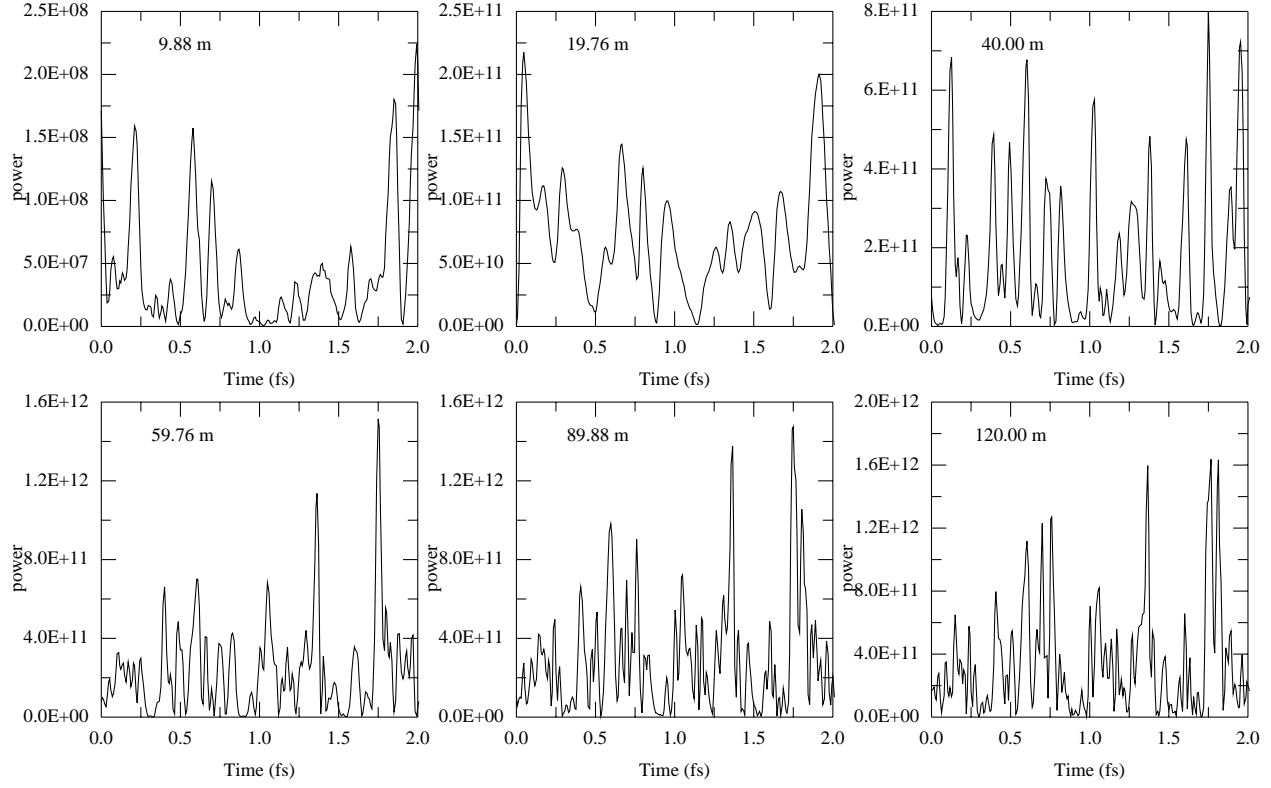


Figure 7. Snapshots of instantaneous power versus time at six z locations for a 1-D GINGER simulation starting from shot noise using the LCLS parameters described in Sec. 2.

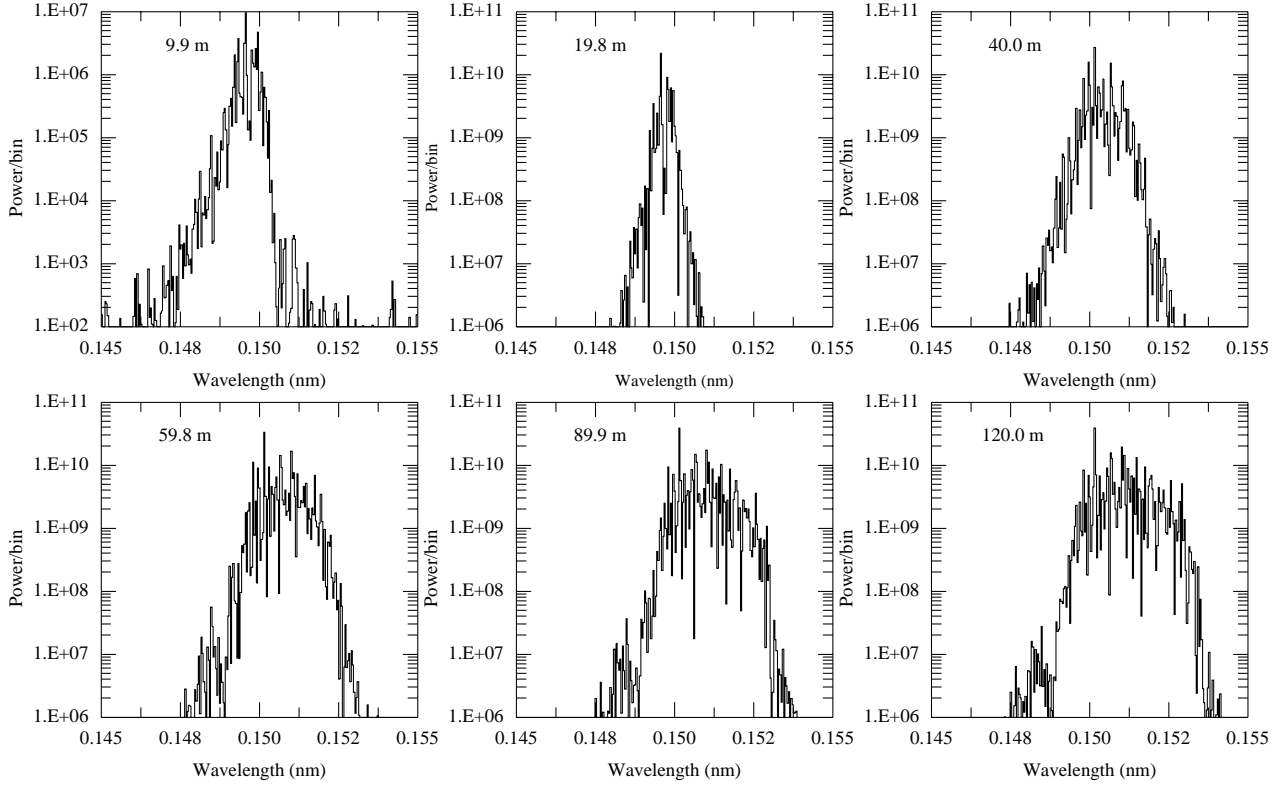


Figure 8. Power spectrum versus wavelength at the same six z -locations of Fig. 7.

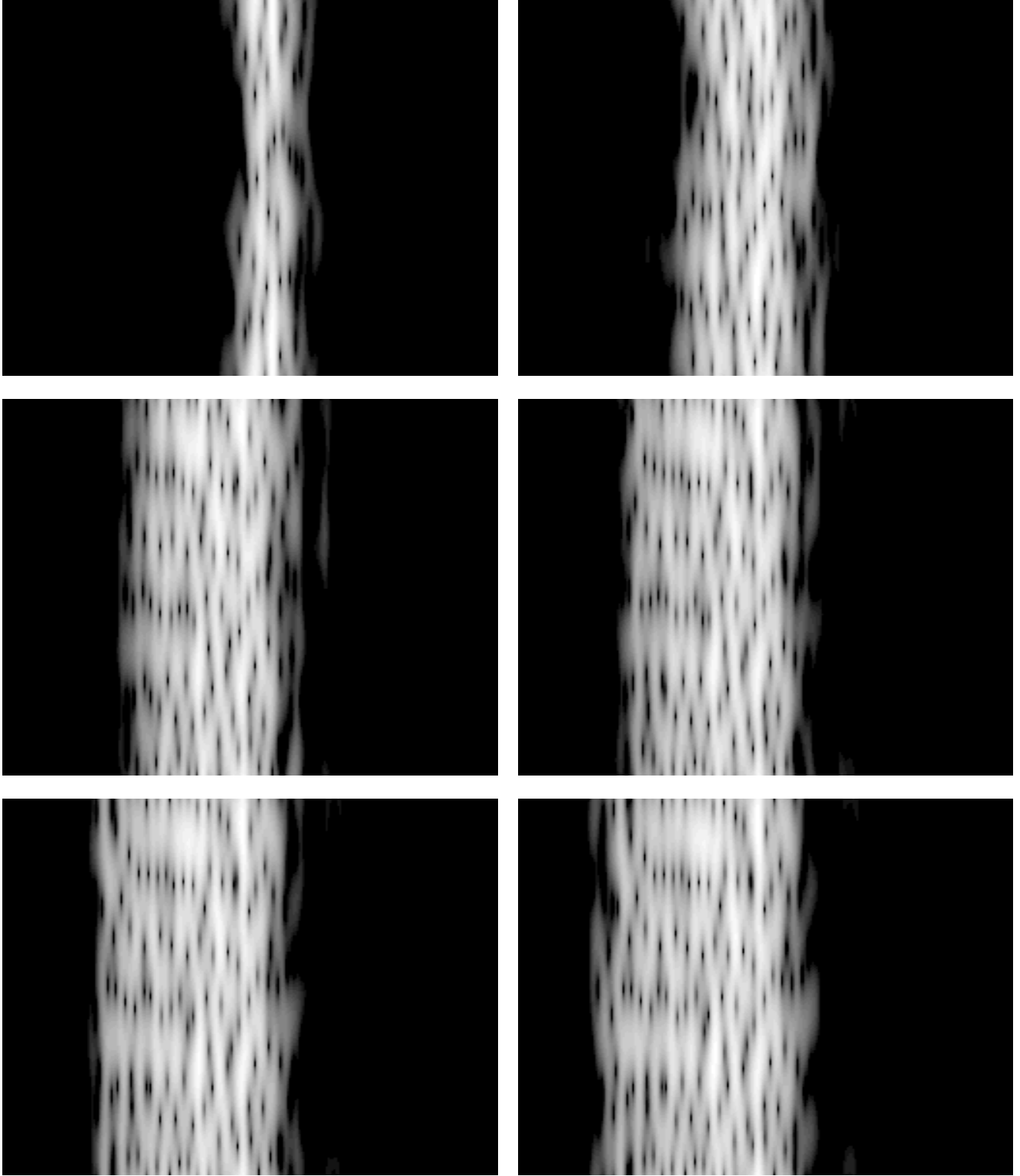


Figure 9. Spectrograms at six z locations spaced evenly from 20 m (top left) to 120 m (bottom right) for the 1-D GINGER run of the previous several figures. Here wavelength runs from right (0.145 nm) to left (0.155 nm) and time from bottom to top in each spectrogram. $S(\omega, \tau)$ is plotted using a logarithmic intensity scale, adopting a floor of $10^{-3} \times S_{max}$.

5. CONCLUSIONS

This paper has investigated various temporal and spectral properties of the output radiation from SASE-initiated short-wavelength FEL's in both the exponential and saturated gain regimes using the GINGER simulation code. The results are in agreement with number of theoretically-predicted properties such as the group velocity of microspike structure in the exponential gain regime and the continued growth of the power in the saturated gain regime. Use of a spectrogram diagnostic shows that in the saturated gain regime the radiation field is composed of discrete "sinews" separated in wavelength, each of whose width is $\sim \rho\lambda_o$. Whether such sinews can be exploited in practice is left as an exercise for the experimentalist.

ACKNOWLEDGEMENTS

The author is pleased to acknowledge numerous useful discussions with P. Pierini, K.-J. Kim, R. Bonifacio, A. Sessler, B. Shadwick, and J. Wurtele. This work was supported by the U.S. Dept. of Energy under Contract DE-AC03-76SF00098. The calculations were done in part using the computational facilities of the U.S. DOE NERSC.

REFERENCES

1. A. M. Kondratenko and E. L. Saldin, "Generation of coherent radiation by a relativistic electron beam in an undulator," *Particle Accelerators* **10**, pp. 207–216, 1980.
2. R. Bonifacio, N. Narducci, and C. Pellegrini, "Collective instabilities and high-gain regime in a free electron laser," *Optics Communications* **50**, pp. 373–378, 1984.
3. K. Kim, "Three-dimensional analysis of coherent amplification and self-amplified spontaneous emission in free-electron lasers," *Physical Review Letters* **57**, pp. 1871–1874, 1986.
4. R. Bonifacio, L. D. Salvo, P. Pierini, N. Piovella, and C. Pellegrini, "Spectrum, temporal structure, and fluctuations in a high-gain free-electron laser starting from noise," *Physical Review Letters* **73**, pp. 70–73, 1994.
5. W. M. Fawley, A. M. Sessler, and E. T. Scharlemann, "Coherence and linewidth studies of a 4-nm high power FEL," in *Proceedings of the 1993 Particle Accelerator Conference, IEEE 93CH3279-7*, pp. 1530–1532, 1993.
6. W. M. Fawley, H.-D. Nuhn, E. Scharlemann, and R. Bonifacio, "Merits of a sub-harmonic approach to a single-pass, 1.5-Angstrom FEL," in *Proceedings of the 1995 Particle Accelerator Conference, IEEE 95CH35843*, p. 269, 1995.
7. P. Pierini and W. M. Fawley, "Shot noise startup of the 6 nm SASE FEL at the TESLA test facility," in *Proceedings of the 17th Int. Free Electron Laser Conf.*, I. Ben-Zvi and S. Krinsky, eds., *Nucl. Instr. Methods Physics Res.* **A375**, pp. 332–335, 1995.
8. R. Tatchyn *et al.*, "Research and development toward a 4.5-1.5Å linac coherent light source (LCLS) at SLAC," in *Proceedings of the 17th Int. Free Electron Laser Conf.*, I. Ben-Zvi and S. Krinsky, eds., *Nucl. Instr. Methods Physics Res.* **A375**, pp. 274–283, 1995.
9. R. A. Jong, W. M. Fawley, and E. T. Scharlemann, "Modelling of induction-linac based free-electron laser amplifiers," in *Modeling and Simulation of Laser Systems, Proc. SPIE* **1045**, pp. 18–27, 1989.
10. K. W. DeLong, D. N. Fittinghoff, and R. Trebino, "Practical issues in ultrashort-laser-pulse measurement using frequency-resolved optical gating," *IEEE J. Quantum Electronics* **32**, pp. 1253–1264, 1996.